Please cite this article in press as: Piatkevich et al., Near-Infrared Fluorescent Proteins Engineered from Bacterial Phytochromes in Neuroimaging, Biophysical Journal (2017), https://doi.org/10.1016/j.bpj.2017.09.007

Biophysical *Journal*
Article

Biophysical Society

Near-Infrared Fluorescent Proteins Engineered from Bacterial Phytochromes in Neuroimaging

Kiryl D. Piatkevich,[1,3] Ho-Jun Suk,[1,2] Suhasa B. Kodandaramaiah,[1,3] Fumiaki Yoshida,[3] Ellen M. DeGennaro,[3,4] Mikhail Drobizhev,[5] Thomas E. Hughes,[5] Robert Desimone,[3,4] Edward S. Boyden,[1,3,4,6,7,*] and Vladislav V. Verkhusha[8,9,*]

[1]Media Lab, [2]Harvard-MIT Division of Health Sciences and Technology, [3]MIT McGovern Institute for Brain Research, and [4]Department of Brain and Cognitive Sciences, MIT, Cambridge, Massachusetts; [5]Department of Cell Biology and Neuroscience, Montana State University, Bozeman, Montana; and [6]Department of Biological Engineering and [7]MIT Center for Neurobiological Engineering, MIT, Cambridge, Massachusetts; and [8]Department of Anatomy and Structural Biology and [9]Gruss-Lipper Biophotonics Center, Albert Einstein College of Medicine, Bronx, New York

ABSTRACT Several series of near-infrared (NIR) fluorescent proteins (FPs) were recently engineered from bacterial phytochromes but were not systematically compared in neurons. To fluoresce, NIR FPs utilize an enzymatic derivative of heme, the linear tetrapyrrole biliverdin, as a chromophore whose level in neurons is poorly studied. Here, we evaluated NIR FPs of the iRFP protein family, which were reported to be the brightest in non-neuronal mammalian cells, in primary neuronal culture, in brain slices of mouse and monkey, and in mouse brain in vivo. We applied several fluorescence imaging modes, such as wide-field and confocal one-photon and two-photon microscopy, to compare photochemical and biophysical properties of various iRFPs. The iRFP682 and iRFP670 proteins exhibited the highest brightness and photostability under one-photon and two-photon excitation modes, respectively. All studied iRFPs exhibited efficient binding of the endogenous biliverdin chromophore in cultured neurons and in the mammalian brain and can be readily applied to neuroimaging.

INRODUCTION

Development of near-infrared (NIR) fluorescent proteins (FPs) is a major focus of the FP engineering field now. Use of NIR light, in comparison to shorter-wavelength light (<640 nm), results in substantially reduced animal tissue absorbance, autofluorescence, and light-scattering. Green fluorescent protein (GFP)-like FPs are widely used in imaging of neurons and in brain in vivo, but their excitation maxima do not exceed 611 nm (1).

Recently, NIR FPs with excitation >640 nm have been engineered from bacterial phytochrome photoreceptors (BphPs) (2,3). BphPs incorporate the most NIR-shifted natural chromophore, a linear tetrapyrrole biliverdin IXα (BV). BV is an enzymatic product of heme breakdown and is naturally present in mammalian cells and tissues. NIR FPs are developed from two N-terminal domains of BphPs, called PAS and GAF (4). The developed NIR FPs exhibit diverse spectral and biochemical properties (Table 1). Specifically, a series of NIR FPs termed iRFP proteins (5–8) spread their fluorescence excitation from 640 to 702 nm and emission from 670 to 720 nm. iRFPs were engineered to bind endogenous BV with high affinity and specificity. In contrast to the iRFP series (5–8), an infrared FP (IFP) series of NIR FPs (9–11), smURFP protein designed from cyanobacterial allophycocyanine (12), and GAF-FP protein designed by truncation of BphP to a single GAF domain (13), require either co-expression of heme oxygenase (HO) or administration of the exogenous BV chromophore or its derivatives to enable their fluorescence in mammalian cells and in vivo. However, HO co-expression and administration of the chromophore can result in cellular artifacts and are impractical. For example, expression of exogenous HO, which plays a crucial role in heme catabolism, can affect cell physiology (14–16). Moreover, co-expression of HO was shown to result in a very modest increase in intracellular brightness of NIR FPs in mammalian cells (17). On the other hand, administration of BV

Submitted May 18, 2017, and accepted for publication September 6, 2017.

*Correspondence: esb@media.mit.edu or vladislav.verkhusha@einstein.yu.edu

Fumiaki Yoshida's present address is Graduate School of Medical Sciences, Kyushu University, Fukuoka, Japan.

Suhasa B. Kodandaramaiah's present address is Department of Mechanical Engineering, University of Minnesota, Minneapolis, Minnesota.

Editor: Vasanthi Jayaraman.

https://doi.org/10.1016/j.bpj.2017.09.007

Please cite this article in press as: Piatkevich et al., Near-Infrared Fluorescent Proteins Engineered from Bacterial Phytochromes in Neuroimaging, Biophysical Journal (2017), https://doi.org/10.1016/j.bpj.2017.09.007

TABLE 1 Spectral and Biochemical Properties of Major NIR FPs Engineered from Bacterial Photoreceptors

NIR FP	Excitation (nm)	Emission (nm)	Molecular Brightness versus iRFP713 (%)[a]	Brightness in HeLa Cells versus iRFP713 (%)[b]	Brightness in Cultured Neurons versus iRFP713 (%)[c]	Photostability in Mammalian Cells, $t_{1/2}$ (s)[d]	Photostability in Cultured Neurons, $t_{1/2}$ (s)[d]	Ref.
iRFP670	643	670	225	119	182	290	64	(7)
iRFP720	702	720	93	110	148	490	178	(7)
iRFP682	663	682	162	105	187	490	173	(7)
iRFP713 (aka iRFP)	690	713	100	100	100	960	333	(5)
iRFP713/V256C	662	680	220	150	ND	ND	ND	(42)
miRFP670	642	670	198	72	ND	155	ND	(8)
iRFP702	673	702	124	61	50	630	154	(7)
miRFP703	674	703	127	37	ND	394	ND	(8)
miRFP709	683	709	69	30	ND	192	ND	(8)
PAiRFP1[e]	659	703	64	25	44	ND	21	(6)
mIFP	683	704	74	14	ND	54	ND	(11)
IFP1.4	684	708	114	8.0	ND	70	ND	(31)
IFP2.0	690	711	80	7.9	ND	108	ND	(10)
PAiRFP2[e]	692	719	60	7	ND	ND	ND	(6)
GAF-FP	635	670	59	2.0	ND	ND	ND	(13)
smURFP	642	670	551	2.0[f]	ND	300	ND	(12)
iBlueberry	644	667	42	ND	ND	954	ND	(43)
BphP1-FP	640	669	126	ND	ND	ND	ND	(44)

Ex, excitation; Em, emission; Ref., reference; ND, not determined.

[a]Molecular brightness is defined as the product of the molar extinction coefficient and the quantum yield of proteins purified from *E. coli*.

[b]Brightness is determined as the effective NIR fluorescence in HeLa cells without exogenous BV and after normalization to the fluorescence of the co-transfected EGFP.

[c]Brightness is determined as the effective NIR fluorescence in live primary mouse hippocampal neurons without exogenous BV and after normalization to the spectrum and power of excitation light, the absorbance of the proteins at the excitation wavelength, and the overlap of the fluorescence spectrum with the transmission of the emission filters and quantum efficiency of the sCMOS camera chip.

[d]The fluorescence decay curves were normalized to absorbance spectra and extinction coefficients of FPs, the spectrum of the lamp, and the transmission of an excitation filter.

[e]PAiRFP2 corresponds to the photoactivated state.

[f]Measured by us without exogenous BV 48 h after the cell transfection.

intravenously is not efficient due to its poor cell-membrane penetration (12).

Despite numerous applications of iRFPs and, to a lesser extent, other NIR FPs in mammalian cells and organs of model animals (3,18), their performance in dissected neurons and in brain has been studied rather poorly.

In this study, we tested the performance of iRFPs in neurons in culture and in vivo without HO co-expression or supplementation of the exogenous chromophore. For this, we selected iRFPs that were reported to efficiently bind endogenous BV and result in the highest NIR fluorescence in cultured mammalian cells among all NIR FPs, namely, iRFP670, iRFP682, iRFP702, iRFP713, and iRFP720 (Table 1). We also studied a photoactivatable iRFP called PAiRFP1, which, unlike photoactivatable GFP-like FPs (19,20), can be photoactivated with far-red light and was chosen as a representative of the photoactivatable iRFPs (6); (Table 1). To express iRFPs in neurons, we used an adeno-associated viral (AAV) expression system (21) and in utero electroporation (IUE) (22). Both methods are widely used to introduce transgenes into neuronal tissue, providing high-level and sustainable protein expression (21,22).

MATERIALS AND METHODS

Molecular cloning

For recombinant adeno-associated virus (rAAV8) production, the corresponding iRFP genes were amplified by polymerase chain reaction and swapped with the tdTomato gene in the pAAV-FLEX-tdTomato plasmid (Addgene: plasmid #28306) using the *Kpn*I and *Bam*HI sites and with the ChR2(H134R)-GFP gene in the pAAV-Syn-ChR2(H134R)-GFP plasmid (Addgene: plasmid #58880) using the *Bam*HI and *Eco*RI sites. Synthetic DNA oligonucleotides used for cloning were purchased from Integrated DNA Technologies (Coralville, IA). PrimeStar Max mastermix (Clontech, Mountain View, CA) was used for high-fidelity polymerase-chain-reaction amplifications. Restriction endonucleases were purchased from New England BioLabs (Ipswich, MA) and used according to the manufacturer's protocols. Ligations were performed using the InFusion HD kit (Clontech). DH5α-competent cells were prepared using the Mix and Go Competent Cells kit (Zymo Research, Irvine, CA). Large-scale DNA plasmid purification was done with the GenElute HP Endotoxin-Free Plasmid Maxiprep Kit (Sigma-Aldrich, St. Louis, MO).

Protein characterization in vitro

Expression and purification of the iRFP proteins were performed as described previously (6), with few modifications. The pBAD/HisB-iRFP670, iRFP682, iRFP702, iRFP713, iRFP720, and PAiRFP1 plasmids (Addgene: 45453, 45454, 45455, 31855, 45460, and 44270, respectively)

Please cite this article in press as: Piatkevich et al., Near-Infrared Fluorescent Proteins Engineered from Bacterial Phytochromes in Neuroimaging, Biophysical Journal (2017), https://doi.org/10.1016/j.bpj.2017.09.007

were co-transformed with pWA23h plasmid, encoding heme oxygenase-1 from *Bradyrhizobium* ORS278 (hmuO) under the rhamnose promoter, into the BW25113 *Escherichia coli* strain (CGSC 7636, Coli Genetic Stock Center, Yale University, New Haven, CT). Bacterial cells were grown in RM medium supplemented with ampicillin, kanamycin, 0.002% arabinose, 0.02% rhamnose for 15–18 h at 37°C and then for 24 h at 18°C. Proteins were purified using TALON metal affinity resin (Clontech) according to the manufacturer's protocol, with one minor modification: in the wash buffer, 100 mM EDTA was used instead of 400 mM imidazole. For absorbance measurements, a Lambda 35 ultraviolet-visible spectrometer (Perkin Elmer, Waltham, MA) was used. Background-light scattering was removed by subtracting a fitted λ^{-4} curve from the measured spectrum.

Two-photon excitation (TPE) spectra and two-photon absorption cross-sections were measured using a PC1 ISS spectrofluorimeter equipped with an NIR-sensitive photomultiplier tube (R928, Hamamatsu, Hamamatsu City, Japan) and operating in photon-counting mode. Two-photon absorption spectra and cross sections of iRFP682 and iRFP713 were measured in phosphate-buffered saline (PBS; pH 7.4) at concentrations of $\sim 1 \times 10^{-4}$ M. The beam from an Insight DeepSee (Newport, Irvine, CA) femtosecond laser, tunable from 680 to 1300 nm, was focused into a 3 × 3 mm cuvette (Starna Cells, Atascadero, CA) and the fluorescence was collected from the first layer (1 mm) of the sample to avoid attenuation of the excitation beam due to water absorption. An optical chopper (1 kHz; Thorlabs, Newton, NJ) and magnetic stirring of the sample solutions were used to minimize the thermal effects.

TPE spectra were recorded using a LabView routine that controlled the step-by-step tuning of the laser. To correct the TPE spectra for the wavelength-to-wavelength variations of laser properties (average power, pulse duration, and beam shape), LDS-798 dye (Exciton Technologies, Edmonton, Alberta, Canada) in deuterated chloroform (Sigma-Aldrich, St. Louis, MO) was used as a reference standard (23). TPE fluorescence had a quadratic dependence on excitation power in the whole spectral range, as presented in the Results (the estimated contribution of one-photon excitation at the power used is <10% in the spectral region 880–900 nm and <2% in the region 900–1300 nm). The two-photon cross section was measured at 1000 nm, using the relative method (24) with LDS-798 in chloroform as a reference standard (23). Fluorescence intensity, F, as a function of excitation power, P, was measured for both the sample and the reference in the same conditions by recording fluorescence at 750 nm. This wavelength was chosen to avoid reabsorption effects while collecting two-photon fluorescence. From the fit of these dependencies to a quadratic function, $F = \alpha P$ (2), factor values were obtained and then normalized to the concentrations (obtained spectrophotometrically with a Lambda 950 spectrophotometer (Perkin Elmer, Waltham, MA)) and differential quantum efficiencies at 750 nm (obtained with an LS-55 spectrofluorimeter (Perkin Elmer)).

Animal care

All methods for animal care and use were approved by the Massachusetts Institute of Technology Committee on Animal Care and were in accordance with the National Institutes of Health Guide for the Care and Use of Laboratory Animals. One adult male rhesus macaque (*Macaca mulatta*) weighing 12 kg was used for this study, as were four PV-Cre × Ai14 (tdTomato) transgenic mice and five Swiss Webster mice, ages ~0–16 weeks. Mice were used without regard to gender.

Primary neuron culture preparation and AAV transduction

Hippocampal neurons were prepared from postnatal day 0 or 1 Swiss Webster mice (Taconic Biosciences, Albany, NY; both male and female mice were used), as previously described (25,26), with the following modifications: dissected hippocampal tissue was digested with 50 units of papain (Worthington Biochemical, Lakewood, NJ) for 6–8 min, and the digestion was stopped with ovomucoid trypsin inhibitor (Worthington Biochemical). Cells were plated at a density of 20,000–30,000 per glass coverslip coated with Matrigel (BD Biosciences, Franklin Lakes, NJ) in standard 24-well plates. Neurons were seeded in 100 μL of plating medium containing minimum essential medium (Life Technologies, Carlsbad, CA), glucose (33 mM; Sigma-Aldrich), transferrin (0.01%; Sigma-Aldrich), Hepes (10 mM; Sigma-Aldrich), Glutagro (2 mM; Corning, Corning, NY), insulin (0.13%; Millipore), B27 supplement (2%; Gibco, Thermo-Fisher Scientific, Waltham, MA), and heat-inactivated fetal bovine serum (7.5%; Corning). After cell adhesion, additional plating medium was added. AraC (0.002 mM; Sigma-Aldrich) was added when glia density was 50–70% of the confluent. Neurons were grown at 37°C and 5% CO_2 in a humidified atmosphere. Cultured neurons were transduced at 4–5 days in vitro (DIV) by rAAV8-Syn-iRFPs (Vector Core, University of North Carolina, Chapel Hill, NC). Briefly, $\sim 10^{10}$ viral particles (the rAAV genome titer was determined by dot blot) per well were used for transduction. All measurements on neurons were taken after DIV 16.

AAV injections

The four 8- to 12-week old PV-Cre × Ai14 (tdTomato) transgenic mice were head-fixed to a stereotaxic apparatus and a small (~0.5 mm^2) craniotomy was performed under continuous isoflurane anesthesia. A 34-gauge injection needle pre-loaded with the rAAV8-FLEX-iRFP (5–10 × 10^{12} particles/mL) was then driven into the brain to a depth of ~400–600 μm from the cortical surface. After injecting 2 μL of the virus mix at 0.2 μL/min, the needle was left at the injection site for an additional 5 min to promote viral diffusion. The animals were allowed to recover from surgery and express the proteins for 4 weeks.

In utero electroporation

An embryonic day 15 timed pregnant female Swiss Webster (Taconic) mouse was deeply anesthetized with 2% isoflurane. Uterine horns were exposed and periodically rinsed with warm PBS. A mixture of pAAV-Syn-iRFP682 and pAAV-CaMKII-Enhanced GFP (EGFP) plasmids at a total DNA concentration of 2 μg/μL was injected into the lateral ventricle of one cerebral hemisphere. Five voltage pulses (50 V, 50 ms duration, 1 Hz) were delivered using the 5 mm round plate electrodes (ECM 830 electroporator; Harvard Apparatus, Holliston, MA). Injected embryos were placed back into the dam, and allowed to mature to delivery.

Mouse perfusion

Deeply anesthetized mice were perfused transcardially with 4% paraformaldehyde in 1 × PBS (pH 7.3) and brains were post-fixed overnight at 4°C. Sections 50 μm thick were cut on a VT1000S vibratome (Leica, Wetzlar, Germany), and mounted in ProLong Antifade Diamond reagent (Invitrogen, Carlsbad, CA).

Macaque procedures

Virus injections were performed with sevoflurane anesthesia using stereotactic coordinates to target eight injection sites. Viruses (rAAV8-Syn-iRFPs) were centrifuged and loaded into 10 μL gas-tight syringes (Hamilton, Reno, NV) that had been back-filled with silicone oil (Sigma-Aldrich). A total of 3 μL of the virus was infused into the brain at two locations (deep, then 500 μm superficial) at a rate of 100−200 nL/min using stereotactic micromanipulator arms (David Kopf Instruments, Los Angeles, CA) and

Please cite this article in press as: Piatkevich et al., Near-Infrared Fluorescent Proteins Engineered from Bacterial Phytochromes in Neuroimaging, Biophysical Journal (2017), https://doi.org/10.1016/j.bpj.2017.09.007

UMP3 micro-syringe injector pumps (World Precision Instruments, Sarasota, FL). After each injection, the needle and syringe were left in place for 10 min before withdrawal. Blunt 33G needles were used for all injections. Dexamethasone (1 mg) was also administered to prevent brain swelling. The animal was perfused 4 weeks after viral injection. An overdose of pentobarbital was administered before perfusion with PBS and 4% paraformaldehyde. The brain was then extracted, blocked, stored in a solution of 20% glycerol and 0.1% sodium azide, and finally cut into 40 μm microtome sections.

Fluorescence microscopy of cultured neurons and fixed brain slices

Fluorescent imaging for Figs. 1 and 2 was performed using a Nikon Eclipse Ti inverted microscope equipped with 40×, NA 1.15 and a 10×, NA 0.45 objectives (Nikon, Tokyo, Japan) and a SPECTRA-X light engine (Lumencor, Beaverton, OR) with 475/28, 585/29, and 631/28 nm exciters (Semrock, Rochester, NY), 660 nm LED (Thorlabs), and a 5.5 Zyla camera

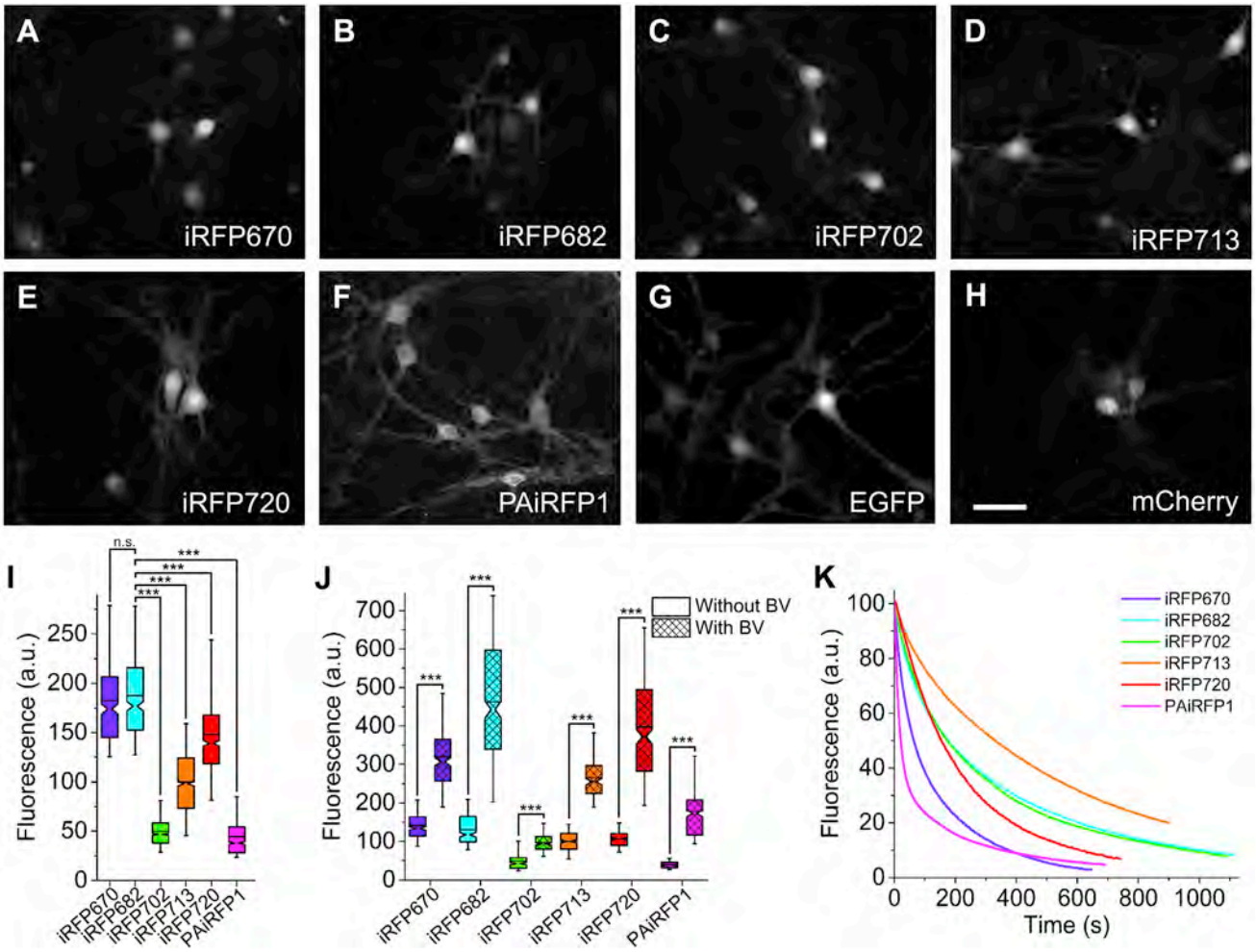

FIGURE 1 Characterization of iRFPs in primary cultured hippocampal mouse neurons. Shown are representative wide-field fluorescence images of cultured neurons at 16 DIV expressing (*A*) iRFP670, (*B*) iRFP682, (*C*) iRFP702, (*D*) iRFP713, (*E*) iRFP720, (*F*) PAiRFP1, (*G*) EGFP, and (*H*) mCherry fluorescent proteins under the control of human synapsin promoter. The images were acquired using 631/28 nm LED light and a 640/14 nm excitation and 676/29 nm emission filter set for iRFP670, and 660/20 nm LED light and a 655/40 nm excitation and 716/40 nm emission filter set for the rest of the iRFPs. The dynamic range for all images was normalized to facilitate visual comparison of protein localization across selected probes (see *I* for fluorescence brightness quantification). Scale bar, 50 μm. (*I*) Relative normalized fluorescence of iRFP670 (*purple*), iRFP682 (*cyan*), iRFP702 (*green*), iRFP713 (*orange*), iRFP720 (*red*), and PAiRFP1 (*magenta*) in cultured neurons (n = 372, 453, 1138, 903, 672, and 840 cells, respectively, from three independent cultures for each protein). Box plots with notches are used throughout this article, where the narrow part of the notch represents the median; the top and bottom of the notch indicate the 95% confidence interval for the median; the top and bottom horizontal lines mark the 25th and 75th percentiles for the data; whiskers extend to the 5th and 95th percentiles for the data; and the black horizontal bar is the mean). $p > 0.05$, not significant (n.s.); ***$p < 0.0001$; one-way analysis of variance followed by post hoc comparisons with a control using Dunnett's method. (*J*) Relative normalized fluorescence of iRFP670 (*purple*), iRFP682 (*cyan*), iRFP702 (*green*), iRFP713 (*orange*), iRFP720 (*red*), and PAiRFP1 (*magenta*) in cultured neurons with (*cross-hatched boxes*) and without (*open boxes*) addition of 25 μM BV for 3 h before imaging (n = 333, 245, 300, 319, 206, 206, 211, 172, 490, 290, 205, and 236 cells, respectively, from one culture). Box plots with notches are used (see caption for (*I*) for description). ***$p < 0.0001$; pairwise one-way analysis of variance. (*K*) Photobleaching curves for iRFP670 (*purple*), iRFP682 (*cyan*), iRFP702 (*green*), iRFP713 (*orange*), iRFP720 (*red*), and PAiRFP1 (*magenta*) in cultured neurons (n = 5, 4, 4, 4, 5, and 4 cells, respectively, from one culture). The curves were normalized to absorbance spectra and extinction coefficients of the proteins, the spectrum of an excitation source, and the transmission of an excitation filter. See Table S1 for full statistics.

Please cite this article in press as: Piatkevich et al., Near-Infrared Fluorescent Proteins Engineered from Bacterial Phytochromes in Neuroimaging, Biophysical Journal (2017), https://doi.org/10.1016/j.bpj.2017.09.007

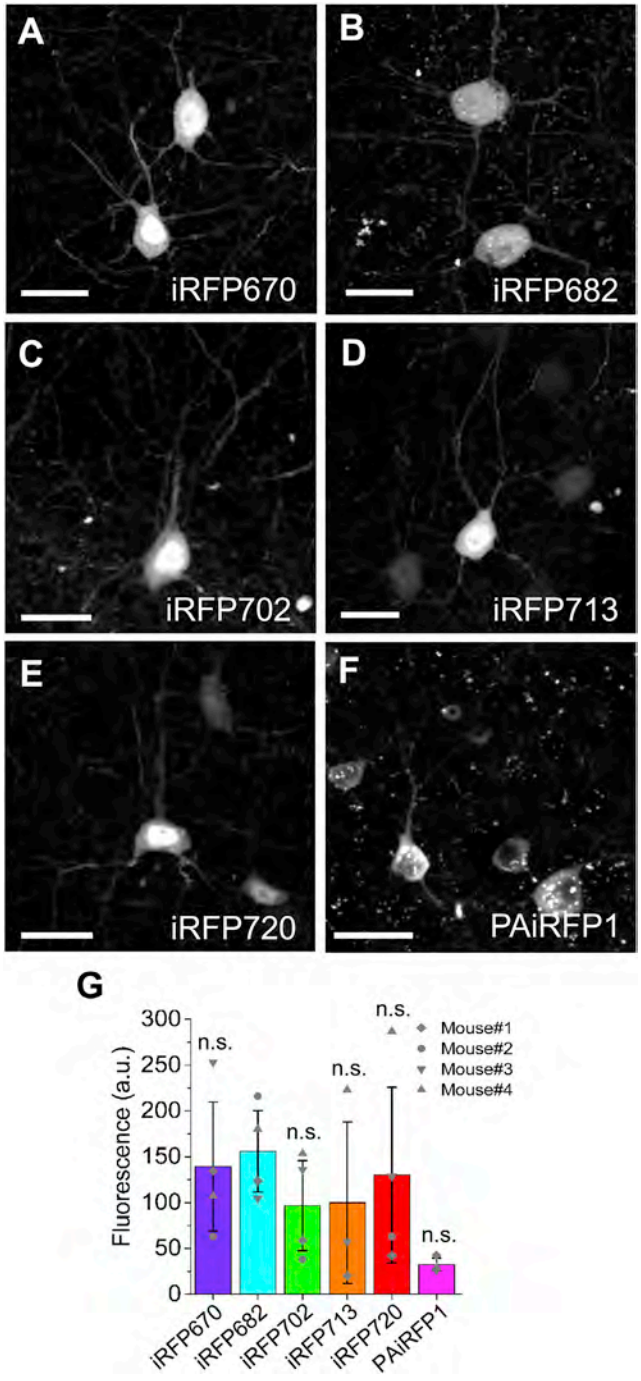

FIGURE 2 Expression of the iRFP proteins in the PV-Cre × Ai14 (tdTomato) transgenic mouse using recombinant AAVs. Representative confocal fluorescence images of cortical neurons expressing (*A*) iRFP670, (*B*) iRFP682, (*C*) iRFP702, (*D*) iRFP713, and (*F*) PAiRFP1; and hippocampal neurons expressing (*E*) iRFP720 (the injection site for iRFP720 unintendedly was ~200 μm deeper than for the other proteins, resulting in expression in the hippocampus) acquired 4 weeks after the corresponding rAAVs injections. The images were acquired using 642 nm laser excitation and a 664 nm long-pass emission filter. The dynamic range for all images was normalized to facilitate visual comparison of protein localization across selected probes (see *G* for NIR fluorescence brightness quantification). Scale bars, 20 μm. (*G*) Mean values of normalized fluorescence intensity of neurons expressing iRFPs (n = 4 mice for iRFP670, iRFP682, iRFP702, and iRFP720; n = 3 mice for iRFP713 and PAiRFP1; gray dots represent individual data points). Mouse 2 had no expression of iRFP713 and PAiRFP1 due to failed AAV injections. n.s., not significant by Kruskal-Wallis analysis. See Table S1 for full statistics. Colored columns with error bars indicate the mean ± SD.

(Andor, Belfast, United Kingdom), controlled by NIS-Elements (Nikon) AR software. Fluorescence imaging for Fig. 3 was performed using an inverted Nikon Eclipse Ti microscope equipped with a spinning disk sCSU-W1 confocal scanner unit (Yokogawa, Tokyo, Japan), 642 nm solid state laser, a 40×, NA 1.15 objective (Nikon), and a 4.2 PLUS Zyla camera (Andor), controlled by NIS-Elements AR software.

Surgical procedures for in vivo imaging

Throughout the surgery, mice were anesthetized with 1–2% (vol/vol) isoflurane in oxygen and maintained at 37°C using a heating pad. After shaving of its scalp, the mouse was placed in a custom-built stereotax, with its eyes covered with ophthalmic ointment. Betadine and 70% ethanol were then applied to the shaved area for sterilization. A polycarbonate recording chamber was implanted in the skull using dental acrylic resin, and a 1–2 mm diameter craniotomy, contained within a 3 mm diameter window of the recording chamber, was made. Right before starting an imaging experiment, 1.5% (v/w) agar in HEPES-buffered artificial cerebrospinal fluid (ACSF; containing 145 mM NaCl, 5.4 mM KCl, 10 mM HEPES, 1.8 mM $CaCl_2$, and 1 mM $MgCl_2$ ((27), pH adjusted to 7.3–7.4 with NaOH) was applied on top of the brain to dampen pulsations caused by respiration and heartbeat, and then the craniotomy was covered with ACSF to keep the brain moist throughout the experiment. We took extra care to minimize bleeding throughout the surgery, as blood on the cortical surface can greatly diminish optical clarity during two-photon imaging (28). In case of bleeding, the brain surface was irrigated with ACSF to stop the bleeding and remove as much blood as possible from the cortical surface. At the end of the experiment, mice were perfused transcardially with 4% paraformaldehyde under anesthesia for subsequent post-mortem analysis of the imaged area.

Two-photon fluorescence microscopy

Two-photon imaging of fixed slices of brain tissue was accomplished using a custom-built microscope system equipped with both a Ti-Sapphire laser (Tsunami; Spectra Physics, Santa Clara, CA) and an optical parametric oscillator (Opal; Spectra Physics) pumped by a second, automatically tunable Ti-Sapphire laser (Mai-Tai; Spectra Physics) (1). This system is thus capable of simultaneously delivering over 100 mW of femtosecond pulsed excitation light in the ranges 780–1040 and 1100–1600 nm. For the simultaneous excitation of tdTomato and iRFP702, the Tsunami and Opal lasers were tuned to 880 and 1280 nm, respectively. Two channels of emission were collected using band-pass filters (Semrock) for red (580/60 nm) and near-infrared (697/75 nm) fluorescence.

For two-photon imaging of iRFPs in cultured neurons and in vivo imaging of EGFP/iRFP682 in mouse, we used a two-photon laser scanning microscope (Ultima IV, Prairie Technologies, Sioux Falls, SD) with a mode-locked Ti-Sapphire laser (Mai-Tai, Spectra Physics) and a water-immersion objective (CFI75 LWD 16×, NA 0.8, working distance, 3.0 mm; Nikon). For image acquisition, the laser was set to emit 880 nm, and 535/50 and 731/137 nm emission filters (Semrock) were used. The microscope was operated using ScanImage 3.8, a MATLAB-based open-source software package (29). ScanImage was configured such that each acquired image had a single frame with 512 lines/frame and 512 pixels/line or 2048 lines/frame and 2048 pixels/line. Each line was scanned in 2.64 ms for a frame rate of 0.74 frames/s (for 512 × 512 images) or 0.18 frames/s (for 2048 × 2048 images).

Please cite this article in press as: Piatkevich et al., Near-Infrared Fluorescent Proteins Engineered from Bacterial Phytochromes in Neuroimaging, Biophysical Journal (2017), https://doi.org/10.1016/j.bpj.2017.09.007

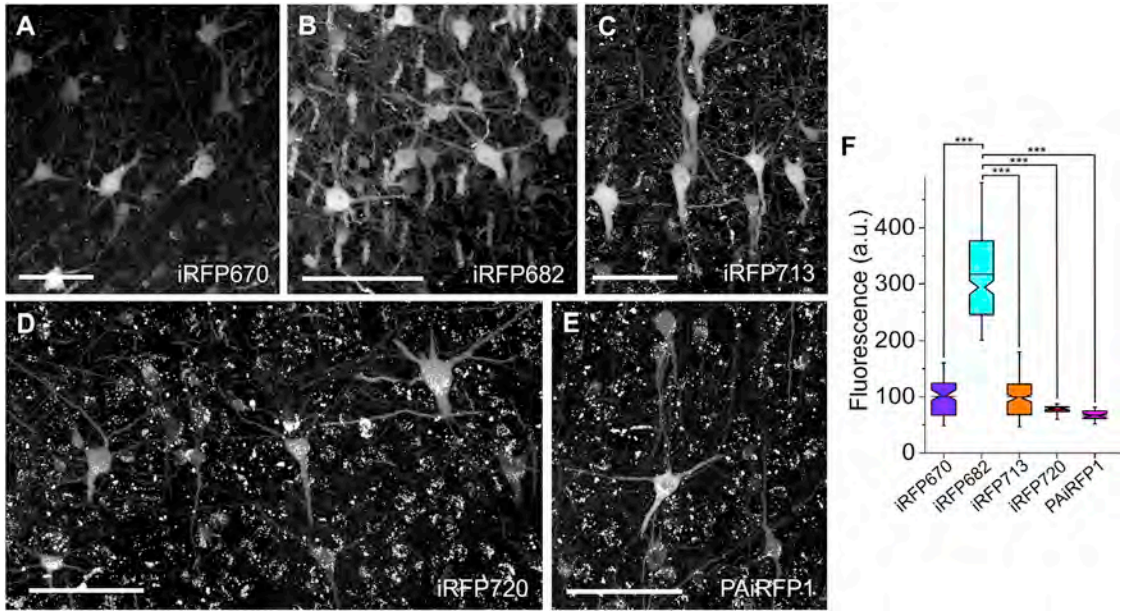

FIGURE 3 Expression of iRFPs in rhesus macaque using recombinant AAVs. Representative confocal fluorescence images of cortical neurons expressing (*A*) iRFP670, (*B*) iRFP682, (*C*) iRFP713, (*D*) iRFP720, and (*E*) PAiRFP1, at 4 weeks after the corresponding rAAVs injections. The fluorescence images were acquired using 642 nm laser excitation and a 664 long-pass emission filter. The dynamic range for all images was normalized to facilitate visual comparison of protein localization across selected proteins (see *F* for NIR fluorescence brightness quantification). Scale bars, 100 μm. (*F*) Relative fluorescence of neurons expressing iRFPs (n = 93, 279, 170, 24, and 27 neurons for iRFP670, iRFP682, iRFP713, iRFP720, and PAiRFP1, respectively). The monkey had no expression of iRFP702 due to the failed virus injection. Box plots with notches are used (see Fig. 1 *I* for a description). ***$p < 0.0001$; nonparametric analysis using Steel with the control method. See Table S1 for full statistics.

Data analysis and statistics

Data were analyzed offline using NIS-Elements Advance Research software, Origin (OriginLab, Northampton, MA), Excel (Microsoft, Redmond, WA), ImageJ, and MATLAB. All statistics were performed in JMP (SAS Institute, Cary, NC).

RESULTS AND DISCUSSION

Characterization of iRFPs in cultured neurons

To evaluate performance of the BphP-based NIR FPs in neurons in vitro, we expressed them by transduction of primary hippocampal mouse neurons with recombinant AAVs serotype 8 (rAAV8) encoding iRFP670, iRFP682, iRFP702, iRFP713, iRFP720, and PAiRFP1 under control of human synapsin promoter (hSyn) and imaged them using wide-field fluorescence microscopy. EGFP and mCherry, expressed under the same conditions as iRFPs, were used as controls for cellular localization. The fluorescence of iRFPs, similar to that observed for EGFP (Fig. 1 *G*), was evenly distributed within the cytosol, individual dendrites, and nucleus of live cultured neurons at 16 DIV without any aggregation or nonspecific localization (Fig. 1, *A–F*). Here and below, the fluorescence of PAiRFP1 was measured after its complete photoactivation either under wide-field illumination with 660/20 nm light of LED or under confocal illumination using a 642 nm laser. Unlike other tested iRFPs, which have a molecular weight of 35 kDa × 2 for a dimer, PAiRFP1, with molecular weight 56.6 kDa × 2 for a dimer, was excluded from the nucleus, most likely due to the decreased passive diffusion through nuclear pores for the larger molecules (30) (Fig. 1 *F*). In contrast to iRFPs and EGFP, mCherry exhibited significant accumulation of fluorescent aggregates in cell bodies (Fig. 1 *H*).

To compare the intracellular brightness of the iRFPs, we quantified NIR of the transduced neurons. To account for different fluorescence spectra of the measured iRFP proteins, throughout this article raw fluorescence intensity values were normalized to spectrum and power of excitation light, absorbance of the proteins at the excitation wavelength, and overlap of the fluorescence spectrum with the transmission of the emission filters and quantum efficiency of the sCMOS camera chip. Normalized mean fluorescence of iRFP670 and iRFP682 over iRFP713 was 1.8-fold higher and statistically significant (Fig. 1 *I*; Table S1). In turn, iRFP720 was 1.5-fold brighter than iRFP713, whereas both iRFP702 and PAiRFP1 exhibited twice lower brightness than iRFP713 (Fig. 1 *I*). Similar to these results obtained in cultured neurons, iRFP670, iRFP682, and iRFP720 were reported to be brighter than iRFP713 in transiently transfected HeLa cells, whereas iRFP702 and PAiRFP1 were dimmer, although relative brightnesses of the tested iRFPs in neurons were different from that measured in HeLa cells (Table 1).

To evaluate the fraction of the iRFP apoproteins in neurons, we compared NIR fluorescence in neurons before

Please cite this article in press as: Piatkevich et al., Near-Infrared Fluorescent Proteins Engineered from Bacterial Phytochromes in Neuroimaging, Biophysical Journal (2017), https://doi.org/10.1016/j.bpj.2017.09.007

and after supplementation with exogenous BV. Administration of saturating concentration of 25 μM BV (31) to the culture medium for 3 h resulted in a 2.3, 3.6, 2.0, 2.7, 3.7, and 4.5-fold increase in NIR fluorescence for iRFP670, iRFP682, iRFP702, iRFP13, iRFP720, and PAiRFP1, respectively (Fig. 1 *J*). This indicates that at least half of the expressed iRFP protein in the AAV-transduced cultured neurons exists in the form of apoprotein.

We next characterized intracellular photostability of the iRFPs in cultured neurons under continuous wide-field excitation light at ~70 mW/mm^2, which is ~2–5 times higher than we typically used for iRFP imaging. Among the tested iRFPs, iRFP713 showed the highest normalized intracellular photostability with photobleaching half-time over 5.5 min, followed by iRFP702, iRFP682, iRFP720, iRFP670, and PAiRFP1 with photostability relative to iRFP713 somewhat reminiscent of what was reported in HeLa cells (6,7); (Fig. 1 *K*; Table 1).

These results showed that the iRFPs can be readily expressed and imaged in cultured neurons without supplementation of exogenous BV or HO-1 co-expression, making these proteins as easy to use as common GFP-like FPs. Good cytoplasmic localization of iRFP682 and iRFP713 in combination with their superior brightness and photostability among tested iRFPs suggests these probes to be preferable for neuronal labeling in NIR range of the spectrum.

Expression of iRFPs in neurons in mouse and monkey

Ability to easily detect expression of the iRFPs in cultured neurons encouraged us to further evaluate their performance in neurons in vivo. First, we expressed selected iRFPs in the cortex of mouse and rhesus macaque by intracranial injections of the rAAV8 vectors. After 4 weeks of expression, fixed brain slices were prepared and analyzed using fluorescence wide-field and confocal microscopy to assess localization and fluorescence brightness of the iRFPs in neurons. Upon expression in the PV-Cre × Ai14 (tdTomato) transgenic mouse, the iRFPs showed good cytoplasmic labeling of parvalbumin interneurons in layer 2/3 of mouse cortex and hippocampal neurons, enabling visualization of somas and individual dendrites (Fig. 2, *A–F*). Fine fluorescent granules of 1–3 μm size, observed both in iRFP682- and PAiRFP1-expressing neurons and outside of them (Fig. 2, *B* and *F*), can be most likely attributed to lipofuscin, an aging pigment that appears to be easily detectable in fixed brain tissue in green, red, and NIR channels due to its wide fluorescence spectrum (32,33); (Fig. S1). Interestingly, when we later expressed iRFP682 in neurons in a mouse via IUE we did not observe lipofuscin granules at the iRFP682-expressing brain region (Fig. 5 *B*), indicating that the observed lipofuscin in Fig. 2 *B* likely is not a result of the iRFP682 expression. Quantification of NIR fluorescence for the tested iRFPs showed that iRFP682 had the highest normalized mean brightness ($n = 4$ mice), which is ~1.6-fold higher than that for iRFP713. In turn, iRFP670 and iRFP720 were 1.4- and 1.3-fold, respectively, brighter than iRFP713, whereas the average fluorescence brightnesses of iRFP702 and PAiRFP1 were 96 and 32%, respectively, of that for iRFP713 (Fig. 2 *G*).

We next studied the behavior of the iRFPs in neurons of monkeys, such as rhesus macaque. All tested iRFPs exhibited good cytoplasmic labeling of cortical neurons in rhesus macaque, allowing visualization of somas and individual dendrites (Fig. 3, *A–E*). Fluorescence intensity of lipofuscin granules in the NIR channel was comparable to that of iRFP670, iRFP713, iRFP720, and PAiRFP1, and could be visualized in the iRFP-expressing neurons and outside of them (Fig. 3, *A* and *C–E*). Similar fluorescence intensity and density of lipofuscin granules were observed for monkey brain tissue injected with EGFP-encoding AAVs (Fig. S2), indicating that iRFP expression did not result in higher lipofuscin formation than EGFP expression. Reminiscent of the results obtained in mouse, iRFP682 demonstrated the highest normalized brightness among all tested iRFPs, with mean fluorescence ~3.2-fold higher than that of iRFP713 (Fig. 3 *F*). iRFP670 and iRFP713 had similar brightness, and iRFP702 and PAiRFP1 were 1.3- and 1.5-fold dimmer than iRFP713.

These results showed that all tested iRFPs can be readily expressed in neurons in vivo in mouse and monkey, and their fluorescence can be easily detected in brain tissue after paraformaldehyde fixation. Quantification of NIR fluorescence suggested that iRFP682 is a preferable NIR genetically encoded probe for neuron labeling.

Two-photon fluorescence microscopy of iRFPs

The BphP-based NIR FPs have already proved to be useful probes for whole-body and deep-tissue imaging of live mammals using one-photon fluorescence microscopy (5–7) and photoacoustic tomography (34,35). We decided to explore performance of the iRFPs under two-photon excitation microscopy, which is also widely used for intravital imaging with subcellular resolution (36). First, to identify an optimal wavelength for TPE, we measured two-photon cross-sections of the iRFPs in the range 880–1300 nm. Two-photon absorption spectra of all measured iRFPs exhibited considerably larger absolute cross-sectional values near the so-called Soret absorbance band (~180–450 GM at 890–950 nm) than near the so-called Q band (~30–70 GM at 1200–1280 nm) (Fig. 4, *A–F*). The iRFP proteins showed similar or lower two-photon brightness compared to that of common red FPs of the GFP-like family (Table S2). Two-photon absorption spectra of iRFPs are similar in shape to porphyrins in the sense that the short-wavelength transition (near the Soret band) is considerably enhanced compared to the long-wavelength transition (near the Q-band). In the case of

Please cite this article in press as: Piatkevich et al., Near-Infrared Fluorescent Proteins Engineered from Bacterial Phytochromes in Neuroimaging, Biophysical Journal (2017), https://doi.org/10.1016/j.bpj.2017.09.007

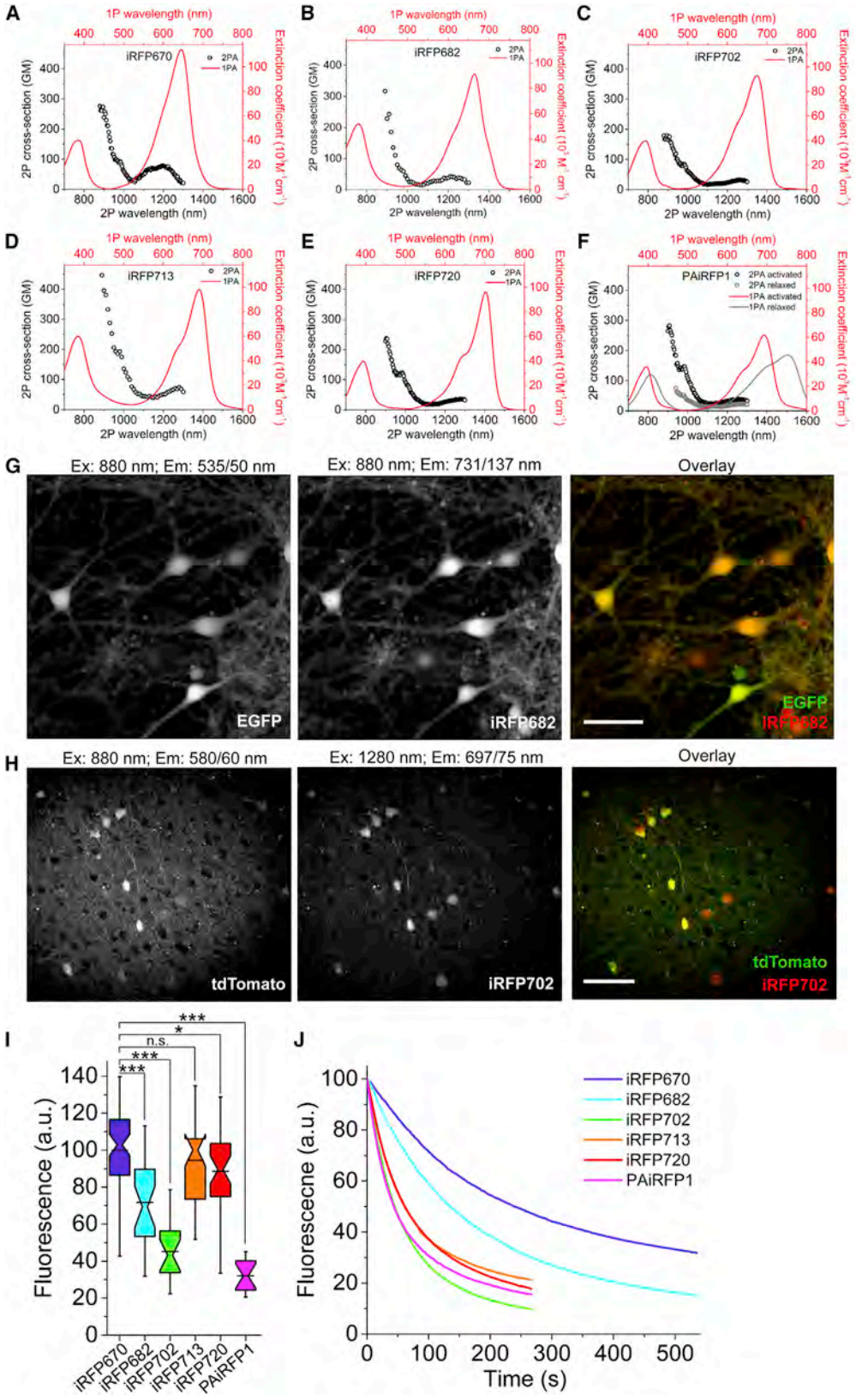

FIGURE 4 Two-photon fluorescence microscopy of iRFPs. One-photon (*solid line*) and two-photon (*open circles*) absorption spectra of (*A*) iRFP670, (*B*) iRFP682, (*C*) iRFP702, (*D*) iRFP713, (*E*) iRFP720, and (*F*) PAiRFP1 in relaxed and activated forms. Two-photon absorption spectra are presented versus laser wavelength used for excitation. GM, Goeppert-Mayer units. (*G*) Two-photon fluorescence images of cultured neurons co-expressing EGFP (left) and

(legend continued on next page)

Please cite this article in press as: Piatkevich et al., Near-Infrared Fluorescent Proteins Engineered from Bacterial Phytochromes in Neuroimaging, Biophysical Journal (2017), https://doi.org/10.1016/j.bpj.2017.09.007

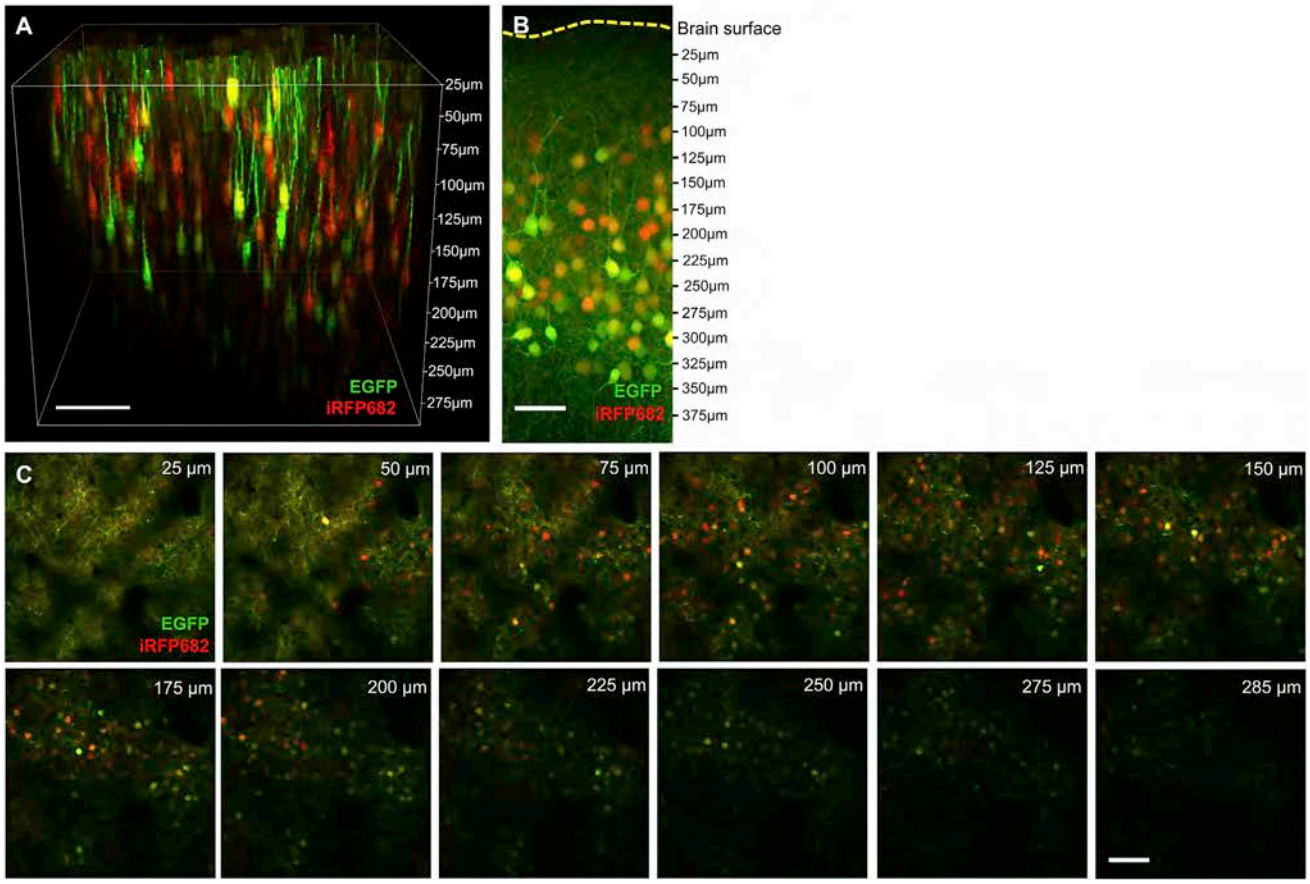

FIGURE 5 In vivo two-photon microscopy of EGFP- and iRFP682-expressing neurons in mouse cortex. (*A*) Volume rendering of two-photon microscopy images of EGFP- and iRFP682-expressing neurons in layer 1 and layer 2/3 of mouse cortex. Images were acquired with 880 nm excitation (6.5 mW) and 535/50 and 731/137 nm emission filters for EGFP and iRFP682, respectively. Scale bars, 100 μm. (*B*) Confocal images of a fixed brain slice corresponding to the region shown in (*A*). Images were acquired using 488 nm laser excitation and 525/50 BP emission for the green channel (EGFP; *green*) and 637 nm laser excitation and a 664 nm long-pass emission filter for the NIR channel (iRFP682; *red*). Scale bars, 50 μm. (*C*) Z-series of images from the stack shown in (*A*). Scale bars, 100 μm.

porphyrins, this was explained before by a resonance enhancement in the three-level system (37). Importantly, the substantial overlap of two-photon cross-sections of iRFPs and EGFP (38) in the range 890–920 nm suggested the possibility of single-wavelength two-photon imaging of both FPs using standard Ti-Sapphire lasers (Fig. S3). Indeed, we were able to perform dual-color imaging of primary neurons co-expressing EGFP and either iRFP682 or iRFP713 using a single excitation wavelength at 880 nm with total light power of 4.05 mW (Figs. 4 *G* and S4). Although we were able to excite the iRFPs in fixed brain tissue under 1280 nm, which corresponds to the Q absorbance band of the BV chromophore, the power level required to achieve sufficient brightness was orders of magnitude higher than that for 880 nm excitation (Fig. 4 *H*). Therefore, for further characterization of iRFPs in a two-photon mode, we decided to use 880 nm two-photon excitation wavelength.

Next, we measured two-photon brightness and photostability of iRFPs expressed in cultured neurons under excitation light power similar to what we usually use for in vivo imaging. Quantification of NIR fluorescence intensity revealed that iRFP670 and iRFP713 had similar brightness, whereas iRFP682, the brightest iRFP under one-photon excitation, was 1.3-fold dimmer than iRFP713 (Fig. 4 *I*). In turn, iRFP720 was only 1.1-fold dimmer than iRFP713, whereas iRFP702 and the photoactivated form of PAiRFP1 exhibited 2.2- and 3.1-fold lower brightness, respectively, than iRFP713 (Fig. 4 *I*). Interestingly, though least

iRFP682 (middle) under 880 nm excitation (right, overlay). Scale bar, 50 μm. (*H*) Two-photon fluorescence images of fixed mouse brain slices co-expressing tdTomato (left) and iRFP702 (middle) under 880 nm (20 mW) and 1280 nm (290 mW) two-photon excitation, respectively (right, overlay). Scale bar, 100 μm. (*I*) Relative normalized fluorescence and (*J*) raw photobleaching curves for iRFP670 (*purple*), iRFP682 (*cyan*), iRFP702 (*green*), iRFP713 (*orange*), iRFP720 (*red*), and PAiRFP1 (*magenta*) in cultured neurons (n = 69, 26, 18, 37, 37, and 14 cells, respectively, from one culture) under 880 nm two-photon excitation and 4.05 mW of total light power. Box plots with notches are used (see Fig. 1 for description). $p > 0.05$, not significant (n.s.); *$p < 0.05$;***$p < 0.0001$; one-way analysis of variance followed by *post-hoc* comparisons with a control using Dunnett's method. See Table S1 for full statistics.

photostable under one-photon excitation among permanently fluorescent iRFPs tested in this study (Fig. 1 *K*), iRFP670 exhibited the highest intracellular two-photon photostability with a photobleaching half-time of 240 s, which is ~3.9-fold higher than that for iRFP713 (Fig. 4 *J*). iRFP682 also outperformed iRFP713 in terms of two-photon photostability, exhibiting a photobleaching rate 2.2-fold slower than that of iRFP713. In turn, iRFP720 had photostability similar to that of iRFP713, and both iRFP702 and the photoactivated form of PAiRFP1 were ~1.4-fold less photostable than iRFP713 (Fig. 4 *J*). Thus, among all tested iRFPs, iRFP670 possessed the best combination of two-photon intracellular brightness and photostability in cultured neurons. In addition, these results clearly demonstrate that two-photon characteristics of the iRFP variants cannot be predicted from their one-photon fluorescence properties and should be carefully measured to select an optimal variant for two-photon excitation microscopy.

Overall, measured biophysical and biochemical characteristics suggest that iRFPs can be used for in vivo two-color imaging in combination with GFP using a standard Ti-Sapphire laser. To test this possibility, we decided to use iRFP682, which, although it possesses lower two-photon brightness and photostability than iRFP670, was shown to have a superior expression in vivo, a beneficial feature for subsequent post mortem analysis of the brain tissue. For this, we co-expressed EGFP and iRFP682 in layer 2/3 of the primary somatosensory cortex by IUE and imaged them in the mouse in vivo at P19 through a cranial window. One can see that the low-level two-photon excitation power of 6.5 mW at 880 nm allowed us to perform dual-color imaging of both FPs as deep as 285 μm from the brain surface with subcellular resolution (Fig. 5). These results suggest that iRFPs, in particular, iRFP670 and iRFP682, due to the superior characteristics can serve as the guide stars for adaptive optics two-photon imaging of GFP-based biosensors of neuronal activity (39) and the fusion tag for safe opsin visualization in brain tissue (40). Moreover, due to its spectral compatibility with GFP-like red FPs with large Stokes shift, such as LSSmKates (36) and CyOFP (41), it can be used for multicolor two-photon imaging with single-wavelength excitation.

As a conclusion, the comprehensive side-by-side comparison of the iRFP series of NIR FPs engineered from BphPs has revealed that they exhibit efficient binding of the endogenous BV chromophore both in cultured primary neurons and in vivo and can be readily applied to neuroimaging. The endogenous concentration of BV chromophore in the brain of mouse and monkey is sufficient to enable NIR fluorescence of the tested iRFPs. Among the iRFPs tested in this study, the iRFP682 and iRFP670 proteins, which exhibit the highest normalized intracellular brightness and photostability in neurons under one-photon excitation and TPE, respectively, are our current NIR FPs of choice for neuroimaging, depending on the imaging modality to be used.

SUPPORTING MATERIAL

Four figures and two tables are available at http://www.biophysj.org/biophysj/supplemental/S0006-3495(17)31018-4.

AUTHOR CONTRIBUTIONS

K.D.P. characterized iRFPs in cultured neurons. M.D. and T.E.H. measured two-photon spectra. K.D.P., S.B.K., and H.-J.S. carried out mouse surgeries. F.Y. carried out primate surgeries under supervision of R.D. and with assistance from E.M.D. H.-J.S. and K.D.P. performed two-photon imaging. K.D.P. and E.S.B. planned experiments and, together with V.V.V., analyzed results. K.D.P. and V.V.V. wrote the manuscript. All authors reviewed and discussed the manuscript.

ACKNOWLEDGMENTS

We thank Nikita Pak (Massachusetts Institute of Technology (MIT)) for help with mouse perfusion and slice preparation, Siranush Babakhanova (MIT) for help with statistical analysis, Demian Park (MIT) for preparation of the primary neuron culture; Rosana Molina (Montana State University) for help with two-photon spectra measurements; and Dave Entenberg (Albert Einstein College of Medicine) for two-photon imaging of iRFP702 in brain slices.

This work was supported by National Institutes of Health grants GM122567, NS099573, and NS103573 (all to V.V.V.), NS094246 (to M.D. and T.E.H.), DA029639, GM104948, and EY023173 (all to E.S.B.), and by a New York Stem Cell Foundation Robertson Award and a Howard Hughes Medical Institute Simons Faculty Scholars grant (both to E.S.B.). H-J.S. was supported by a Samsung Fellowship.

REFERENCES

1. Morozova, K. S., K. D. Piatkevich, …, V. V. Verkhusha. 2010. Far-red fluorescent protein excitable with red lasers for flow cytometry and superresolution STED nanoscopy. *Biophys. J.* 99:L13–L15.
2. Shcherbakova, D. M., A. A. Shemetov, …, V. V. Verkhusha. 2015. Natural photoreceptors as a source of fluorescent proteins, biosensors, and optogenetic tools. *Annu. Rev. Biochem.* 84:519–550.
3. Chernov, K. G., T. A. Redchuk, …, V. V. Verkhusha. 2017. Near-infrared fluorescent proteins, biosensors, and optogenetic tools engineered from phytochromes. *Chem. Rev.* 117:6423–6446.
4. Piatkevich, K. D., F. V. Subach, and V. V. Verkhusha. 2013. Engineering of bacterial phytochromes for near-infrared imaging, sensing, and light-control in mammals. *Chem. Soc. Rev.* 42:3441–3452.
5. Filonov, G. S., K. D. Piatkevich, …, V. V. Verkhusha. 2011. Bright and stable near-infrared fluorescent protein for in vivo imaging. *Nat. Biotechnol.* 29:757–761.
6. Piatkevich, K. D., F. V. Subach, and V. V. Verkhusha. 2013. Far-red light photoactivatable near-infrared fluorescent proteins engineered from a bacterial phytochrome. *Nat. Commun.* 4:2153.
7. Shcherbakova, D. M., and V. V. Verkhusha. 2013. Near-infrared fluorescent proteins for multicolor in vivo imaging. *Nat. Methods.* 10:751–754.
8. Shcherbakova, D. M., M. Baloban, …, V. V. Verkhusha. 2016. Bright monomeric near-infrared fluorescent proteins as tags and biosensors for multiscale imaging. *Nat. Commun.* 7:12405.
9. Shu, X., A. Royant, …, R. Y. Tsien. 2009. Mammalian expression of infrared fluorescent proteins engineered from a bacterial phytochrome. *Science.* 324:804–807.
10. Yu, D., W. C. Gustafson, …, X. Shu. 2014. An improved monomeric infrared fluorescent protein for neuronal and tumour brain imaging. *Nat. Commun.* 5:3626.

11. Yu, D., M. A. Baird, …, X. Shu. 2015. A naturally monomeric infrared fluorescent protein for protein labeling in vivo. *Nat. Methods.* 12:763–765.
12. Rodriguez, E. A., G. N. Tran, …, R. Y. Tsien. 2016. A far-red fluorescent protein evolved from a cyanobacterial phycobiliprotein. *Nat. Methods.* 13:763–769.
13. Rumyantsev, K. A., D. M. Shcherbakova, …, V. V. Verkhusha. 2015. Minimal domain of bacterial phytochrome required for chromophore binding and fluorescence. *Sci. Rep.* 5:18348.
14. Takeda, A., G. Perry, …, M. A. Smith. 2000. Overexpression of heme oxygenase in neuronal cells, the possible interaction with Tau. *J. Biol. Chem.* 275:5395–5399.
15. Song, W., H. Su, …, H. M. Schipper. 2006. Over-expression of heme oxygenase-1 promotes oxidative mitochondrial damage in rat astroglia. *J. Cell. Physiol.* 206:655–663.
16. Chen, K., K. Gunter, and M. D. Maines. 2000. Neurons overexpressing heme oxygenase-1 resist oxidative stress-mediated cell death. *J. Neurochem.* 75:304–313.
17. Shemetov, A. A., O. S. Oliinyk, and V. V. Verkhusha. 2017. How to increase brightness of near-infrared fluorescent proteins in mammalian cells. *Cell Chem. Biol.* 24:758–766.e3.
18. Shcherbakova, D. M., M. Baloban, and V. V. Verkhusha. 2015. Near-infrared fluorescent proteins engineered from bacterial phytochromes. *Curr. Opin. Chem. Biol.* 27:52–63.
19. Piatkevich, K. D., and V. V. Verkhusha. 2010. Advances in engineering of fluorescent proteins and photoactivatable proteins with red emission. *Curr. Opin. Chem. Biol.* 14:23–29.
20. Wu, B., K. D. Piatkevich, …, V. V. Verkhusha. 2011. Modern fluorescent proteins and imaging technologies to study gene expression, nuclear localization, and dynamics. *Curr. Opin. Cell Biol.* 23:310–317.
21. Betley, J. N., and S. M. Sternson. 2011. Adeno-associated viral vectors for mapping, monitoring, and manipulating neural circuits. *Hum. Gene Ther.* 22:669–677.
22. Saito, T., and N. Nakatsuji. 2001. Efficient gene transfer into the embryonic mouse brain using in vivo electroporation. *Dev. Biol.* 240:237–246.
23. Makarov, N. S., J. Campo, …, J. W. Perry. 2011. Rapid, broadband two-photon-excited fluorescence spectroscopy and its application to red-emitting secondary reference compounds. *Opt. Mater. Express.* 1:551.
24. Makarov, N. S., M. Drobizhev, and A. Rebane. 2008. Two-photon absorption standards in the 550–1600 nm excitation wavelength range. *Opt. Express.* 16:4029–4047.
25. Chow, B. Y., X. Han, …, E. S. Boyden. 2010. High-performance genetically targetable optical neural silencing by light-driven proton pumps. *Nature.* 463:98–102.
26. Klapoetke, N. C., Y. Murata, …, E. S. Boyden. 2014. Independent optical excitation of distinct neural populations. *Nat. Methods.* 11:338–346.
27. Chen, I.-W., F. Helmchen, and H. Lütcke. 2015. Specific early and late oddball-evoked responses in excitatory and inhibitory neurons of mouse auditory cortex. *J. Neurosci.* 35:12560–12573.
28. Komai, S., W. Denk, …, T. W. Margrie. 2006. Two-photon targeted patching (TPTP) in vivo. *Nat. Protoc.* 1:647–652.
29. Pologruto, T. A., B. L. Sabatini, and K. Svoboda. 2003. ScanImage: flexible software for operating laser scanning microscopes. *Biomed. Eng. Online.* 2:13.
30. Timney, B. L., B. Raveh, …, M. P. Rout. 2016. Simple rules for passive diffusion through the nuclear pore complex. *J. Cell Biol.* 215:57–76.
31. Makarov, V., G. Manina, …, S. T. Cole. 2009. Benzothiazinones kill mycobacterium tuberculosis by blocking arabinan synthesis. *Science.* 324:801–804.
32. Schnell, S. A., W. A. Staines, and M. W. Wessendorf. 1999. Reduction of lipofuscin-like autofluorescence in fluorescently labeled tissue. *J. Histochem. Cytochem.* 47:719–730.
33. Croce, A. C., and G. Bottiroli. 2014. Autofluorescence spectroscopy and imaging: a tool for biomedical research and diagnosis. *Eur. J. Histochem.* 58:2461.
34. Filonov, G. S., A. Krumholz, …, V. V. Verkhusha. 2012. Deep-tissue photoacoustic tomography of a genetically encoded near-infrared fluorescent probe. *Angew. Chem. Int. Ed. Engl.* 51:1448–1451.
35. Krumholz, A., D. M. Shcherbakova, …, V. V. Verkhusha. 2014. Multicontrast photoacoustic in vivo imaging using near-infrared fluorescent proteins. *Sci. Rep.* 4:3939–3943.
36. Piatkevich, K. D., J. Hulit, …, V. V. Verkhusha. 2010. Monomeric red fluorescent proteins with a large Stokes shift. *Proc. Natl. Acad. Sci. USA.* 107:5369–5374.
37. Karotki, A.…, 2003. Enhancement of two-photon absorption in tetrapyrrolic compounds. *J. Opt. Soc. Am. B.* 20:321.
38. Drobizhev, M., N. S. Makarov, …, A. Rebane. 2011. Two-photon absorption properties of fluorescent proteins. *Nat. Methods.* 8:393–399.
39. Wang, K., W. Sun, …, N. Ji. 2015. Direct wavefront sensing for high-resolution in vivo imaging in scattering tissue. *Nat. Commun.* 6:7276.
40. Richie, C. T., L. R. Whitaker, …, B. K. Harvey. 2017. Near-infrared fluorescent protein iRFP713 as a reporter protein for optogenetic vectors, a transgenic Cre-reporter rat, and other neuronal studies. *J. Neurosci. Methods.* 284:1–14.
41. Chu, J., Y. Oh, …, M. Z. Lin. 2016. A bright cyan-excitable orange fluorescent protein facilitates dual-emission microscopy and enhances bioluminescence imaging in vivo. *Nat. Biotechnol.* 34:760–767.
42. Stepanenko, O. V., M. Baloban, …, V. V. Verkhusha. 2016. Allosteric effects of chromophore interaction with dimeric near-infrared fluorescent proteins engineered from bacterial phytochromes. *Sci. Rep.* 6:18750.
43. Yu, D., Z. Dong, …, X. Shu. 2016. Rational design of a monomeric and photostable far-red fluorescent protein for fluorescence imaging in vivo. *Protein Sci.* 25:308–315.
44. Shcherbakova, D. M., M. Baloban, …, V. V. Verkhusha. 2015. Molecular basis of spectral diversity in near-infrared phytochrome-based fluorescent proteins. *Chem. Biol.* 22:1540–1551.

Biophysical Journal, Volume *113*

Supplemental Information

Near-Infrared Fluorescent Proteins Engineered from Bacterial Phytochromes in Neuroimaging

Kiryl D. Piatkevich, Ho-Jun Suk, Suhasa B. Kodandaramaiah, Fumiaki Yoshida, Ellen M. DeGennaro, Mikhail Drobizhev, Thomas E. Hughes, Robert Desimone, Edward S. Boyden, and Vladislav V. Verkhusha

Figure 1S.

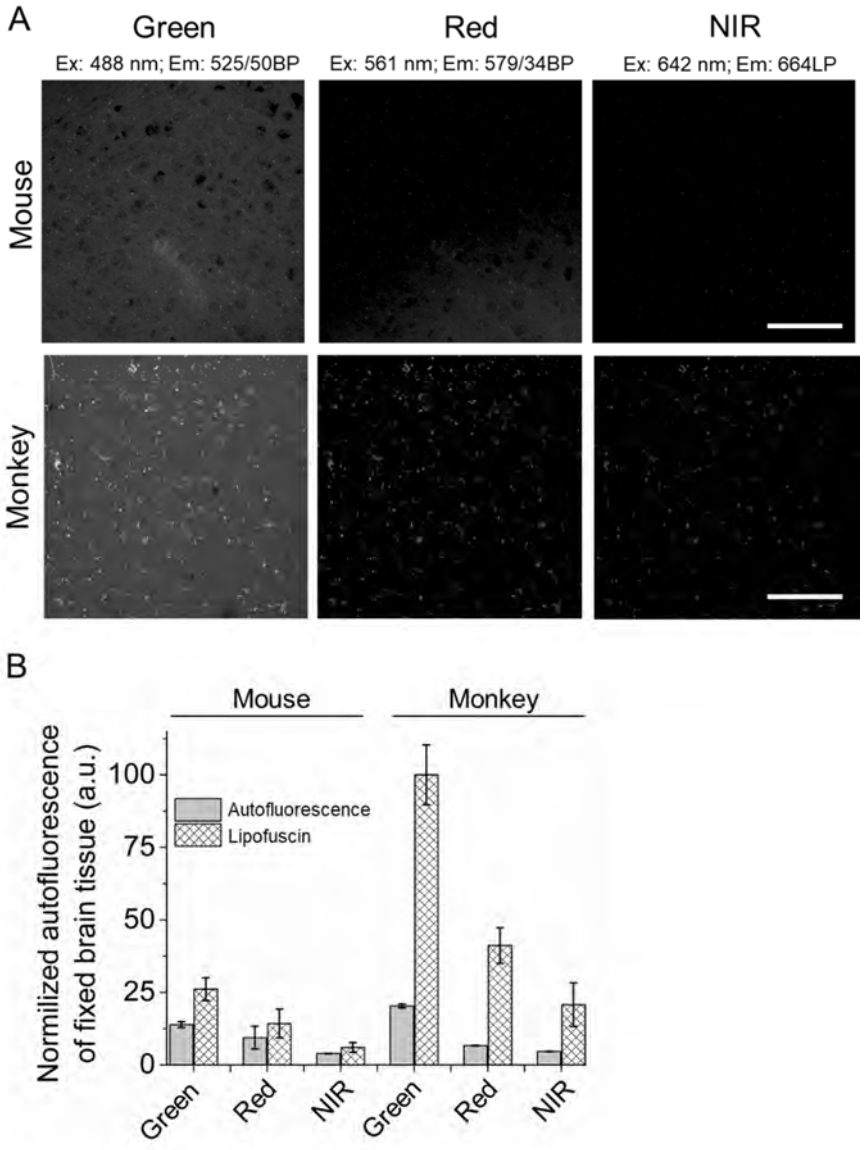

(**A**) Representative fluorescence confocal images of fixed mouse (upper raw) and (lower raw) monkey brain slices in green, red, and NIR channels. All images were acquired at the same exposure time, camera binning, and excitation light power (29 mW/mm^2), and are presented in the same dynamic range. Lipofuscin granules can be easily visualized in monkey brain tissue in all three channels. Scale bar, 100 μm. (**B**) Relative normalized autofluorescence (not including lipofuscin fluorescence; gray columns) and lipofuscin fluorescence (crosshatched columns) of fixed mouse and monkey brain tissue, quantified from the experiment shown in panel **A** (n = 4 fields of view of cortext for each sample).

Figure 2S.

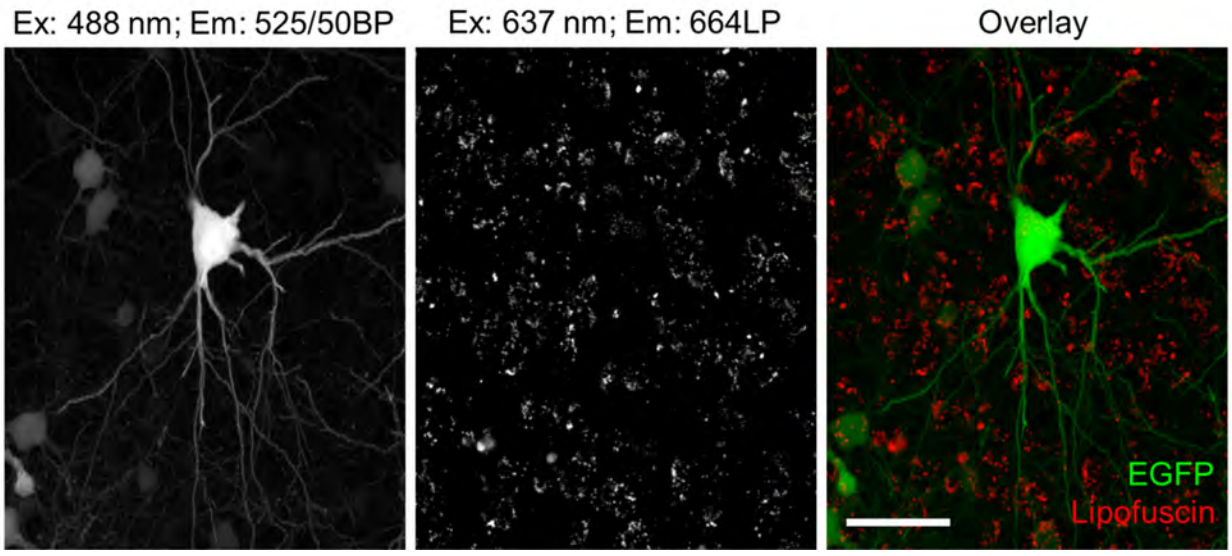

Representative fluorescence confocal images of fixed monkey brain slice expressing EGFP in neurons. Lipofuscin granules can be easily visualized in NIR channel used for iRFP imaging. Scale bar, 5 μm.

Figure 3S.

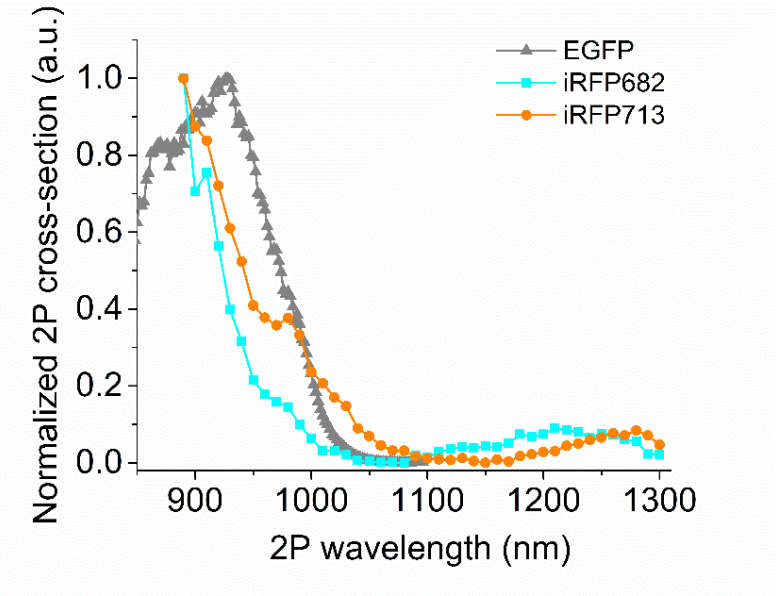

Overlay of the normalized two-photon absorption spectra of EGFP (gray triangular), iRFP682 (cyan squares), and iRFP713 (orange circles). The two-photon absorption spectra of EGFP is adopted from reference [1].

Figure 4S.

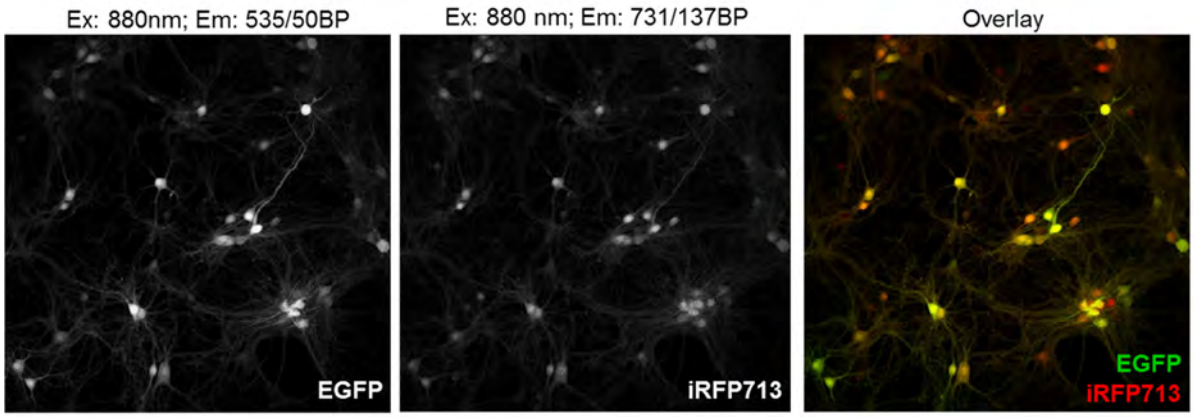

Two-photon fluorescence images of cultured neurons co-expressing EGFP (left) and iRFP713 (middle) under 880 nm excitation (right, overlay). Scale bar, 100 μm.

Table 1S. Statistical analysis for Figures 1, 2 and 3.

Statistical analysis for Fig. 1I.

Protein	Number of data points for statistics (n)	Mean	Standard error of mean
iRFP670	372	182.31	2.60
iRFP682	453	187.50	2.31
iRFP702	1138	49.73	0.49
iRFP713	903	100.00	1.18
iRFP720	672	148.16	1.86
PAiRFP1	840	44.23	0.70

Comparisons with a control using Dunnett's Method.
Control Group: iRFP682.

|d|	Alpha
2.47406	0.05

Protein	Abs(Dif)-LSD	p-Value
iRFP670	-0.88	0.1181
iRFP702	132.9	<0.0001
iRFP713	82.5	<0.0001
iRFP720	34.07	<0.0001
PAiRFP1	138.2	<0.0001

Statistical analysis for Fig. 1J.

Pairwise 1-way Analysis of variance

Protein	Number of data points for statistics (n)	Mean	Standard error of mean
iRFP670 without BV	333	140.56	39.20
iRFP670 with BV	245	319.46	93.00

DF	F Ratio	Prob > F
1	992.87	<0.0001

Protein	Number of data points for statistics (n)	Mean	Standard error of mean
iRFP682 without BV	300	130.10	41.90
iRFP682 with BV	319	462.60	168.95

DF	F Ratio	Prob > F
1	1098.39	<0.0001

Protein	Number of data points for statistics (n)	Mean	Standard error of mean
iRFP702 without BV	206	48.94	23.82
iRFP702 with BV	206	97.39	26.40

DF	F Ratio	Prob > F
1	382.65	<0.0001

Protein	Number of data points for statistics (n)	Mean	Standard error of mean
iRFP713 without BV	211	100.01	28.13
iRFP713 with BV	172	265.37	57.76

DF	F Ratio	Prob > F
1	1340.06	<.0001

Protein	Number of data points for statistics (n)	Mean	Standard error of mean
iRFP720 without BV	490	107.05	24.10
iRFP720 with BV	290	397.55	143.36

DF	F Ratio	Prob > F
1	1921.90	<0.0001

Protein	Number of data points for statistics (n)	Mean	Standard error of mean
PAiRFP1 without BV	205	39.57	9.21
PAiRFP1 with BV	236	178.55	80.67

DF	F Ratio	Prob > F
1	601.52	<0.0001

Statistical analysis for Fig. 2B.

Protein	Number of data points for statistics (n)	Mean	Standard error of mean

iRFP670	372	139.52	40.67
iRFP682	453	156.12	25.67
iRFP702	1138	96.63	28.36
iRFP713	903	100.00	62.45
iRFP720	672	130.07	55.39
PAiRFP1	840	32.49	5.06

Kruskal-Wallis Test Rank Sums.

Protein	**Count**	**Score Sum**	**Expected Score**	**Score Mean**	**(Mean-Mean0)/Std0**
iRFP670	4	58.000	46.000	14.5000	0.979
iRFP682	4	61.000	46.000	15.2500	1.234
iRFP702	4	45.000	46.000	11.2500	-0.043
iRFP713	3	28.000	34.500	9.3333	-0.574
iRFP720	4	50.000	46.000	12.5000	0.298
PAiRFP1	3	11.000	34.500	3.6667	-2.200

Oneay Test, ChiSquare Approximation.

ChiSquare	**DF**	**Prob>ChiSq**
6.9881	5	0.2215

Statistical analysis for Fig. 3.

Protein	**Number of data points for statistics (n)**	**Mean**	**Standard error of mean**
iRFP670	93	100.24	3.88
iRFP682	279	316.65	5.71
iRFP713	170	99.99	2.96
iRFP720	24	76.29	1.84
PAiRFP1	27	66.84	1.72

Nonparametric Comparisons with Control Using Steel Method.
Control Group: iRFP682.

q*	**Alpha**
2.48487	0.05

Protein	**Z**	**p-Value**
iRFP670	14.3987	<0.0001
iRFP713	8.1277	<0.0001
iRFP720	8.5786	<0.0001
PAiRFP1	17.7209	<0.0001

Statistical analysis for Fig. 4.

Protein	Number of data points for statistics (n)	Mean	Standard error of mean
iRFP670	69	100	2.66
iRFP682	26	71.71	4.32
iRFP702	18	45.15	3.71
iRFP713	37	94.62	3.60
iRFP720	37	88.53	3.68
PAiRFP1	14	32.08	2.28

Oneway Anova

Source	DF	Sum of Squares	Mean Square	F Ratio	Prob > F
Molecule	5	91395.92	18279.2	41.4662	<.0001*
Error	195	85960.14	440.8		
C. Total	200	177356.07			

Comparisons with a control using Dunnett's Method
Control Group = iRFP670
Confidence Quantile

|d|	Alpha
2.57745	0.05

LSD Threshold Matrix

Protein	Abs(Dif)-LSD	p-Value
iRFP670	-9.21	1.0000
iRFP682	15.84	<.0001
iRFP702	40.52	<.0001
iRFP713	-5.65	0.6602
iRFP720	0.446	0.0376
PAiRFP1	52.06	<.0001

Table 2S. One-photon and two-photon properties of the representative red fluorescent proteins of GFP-like family and near-infrared fluorescent proteins derived from bacterial phytochromes.

Fluorescent Protein		Abs (nm)	Em (nm)	Molecular brightness	S_0 to S_n transition			S_0 to S_1 transition			Reference
					λ_{2PA} (nm)	σ_2 (GM)	σ_2' (GM)	λ_{2PA} (nm)	σ_2 (GM)	σ_2' (GM)	
TagRFP		555	584	48,000	759	300	130	1,050	95	42	[1]
tdTomato		554	581	48,000	684	316	228	1,050	278	200	[1]
DsRed2		563	582	24,000	700	112	79	1,050	103	73	[1]
mCherry		587	610	16,000	740	101	24	1,080	27	6.4	[1]
mKate2		588	633	25,000	712	216	91	1,140	72	30	[1]
mNeptune		600	650	13,000	750	335	57	1,105	70	12	[1]
iRFP670		645	670	12,650	880[a]	276	31	1,196	78	8.7	this study
iRFP682		670	682	12,600	890[a]	316	35	1,210	43	4.8	this study
iRFP702		674	702	7,620	880[a]	179	15	1,256	33	2.7	this study
iRFP713		692	713	6,200	890[a]	446	28	1,280	74	4.7	this study
iRFP720		702	720	5,760	900[a]	229	14	1,276	38	2.3	this study
PAiRFP1[b]	R	751	NA	NA	940[a]	75	NA	1,284	24	NA	this study
	A	693	717	3,221	900[a]	265	13	1,256	39	1.9	

Abs, one-photon absorption maximum; Em, fluorescence emission maximum; Molecular brightness, a product of molar extinction coefficient and quantum yield; λ_{2PA}, two-photon absorption maximum; σ_2, two-photon absorption cross-section, σ_2, two-photon brightness; GM, units of Goeppert-Mayer where 1 GM is $10^{-50}\cdot cm^4\cdot s\cdot photon^{-1}$. [a] Minimal measured wavelength; [b] PAiRFP1's R and A stand for relaxed and photoactivated forms of the protein, respectively.

Supporting References

1. Drobizhev, M., Makarov, N. S., Tillo, S. E., Hughes, T. E. & Rebane, A. Two-photon absorption properties of fluorescent proteins. *Nat Methods* **8,** 393–399 (2011).